

Identifying an effective model for the two-stage-Kondo regime: Numerical renormalization group results

P. A. Almeida,^{1,2,*} E. Vernek,¹ E. V. Anda,³ S. E. Ulloa,^{2,†} and G. B. Martins^{1,‡}

¹*Instituto de Física, Universidade Federal de Uberlândia, Uberlândia, Minas Gerais 38400-902, Brazil*

²*Department of Physics and Astronomy and Nanoscale and Quantum Phenomena Institute, Ohio University, Athens, Ohio 45701-2979, USA*

³*Departamento de Física, Pontifícia Universidade Católica do Rio de Janeiro (PUC-Rio), Rio de Janeiro, Rio de Janeiro, 22453-900, Brazil*

(Dated: December 10, 2024)

A composite impurity in a metal explores different configurations, where its net magnetic moment may be screened by the electrons in the host. An interesting example is the two-stage Kondo (TSK) system where screening sets in with successively smaller energy scales. In contrast, the impurities may prefer a local singlet disconnected from the metal. This competition is decided by fine-tuning of the couplings in the system, as has been studied before. A double quantum dot T-shape geometry, where a ‘hanging’ dot is connected to current leads only via another dot, represents a flexible system in which these different regimes can be explored experimentally. It has been difficult, however, to clearly differentiate the two regimes. Here, we provide a prescription to better identify the regime where the TSK occurs in such double dot geometry. The TSK regime requires a balance of the ratio t_{01}/Γ_0 between the inter-dot coupling (t_{01}) and the coupling of the QD connected to the Fermi sea (Γ_0). Above a certain value of this ratio, the system crosses over to a molecular regime, where the quantum dots form a local singlet, and no Kondo screening occurs. Here, we establish that there is a region in the $t_{01} - \Gamma_0$ parameter space where a *pure* TSK regime occurs, i.e., where the properties of the second Kondo stage can be accurately described by a single impurity Anderson model with effective/renormalized parameters. By examining the magnetic susceptibility of the hanging QD, we show that a single parameter, Γ_{eff} , can accurately simulate this susceptibility. This *effective* model also provides the hanging QD spectral function with great accuracy in a limited range of the $t_{01} - \Gamma_0$ parameter space, thus defining the region where a true TSK regime occurs. We also show that in this parameter range, the spin correlations between both quantum dots show a universal behavior. Our results may guide experimental groups to choose parameter values that will place the system either in the TSK regime or in the crossover to the molecular regime.

I. Introduction

Point defects in semiconductors—in the form of vacancies, for example—may greatly affect the electrical conductivity of a host crystal [1]. Similarly, magnetic impurities can qualitatively alter the electrical conductivity of their metallic hosts at low temperatures [2]. The former effect, once understood in the 1940s [3], found its first technological applications in the 1950s and ushered the microelectronics revolution. The latter, a much more subtle effect, was first observed in the early 1930s [2], and took three decades to be partially understood [4] as being related to many-body processes. This interesting phenomenon came to be called the Kondo effect [5] and it was modeled in the early 1960s [6] by the single impurity Anderson model (SIAM). It was partially solved in the mid 1960s [4] (through a mapping to the Kondo model [7]), and finally solved and deeply understood at the end of the 1970s through renormalization group ideas [8, 9].

A vacancy in a semiconductor, being a single-electron problem, does not lead to qualitatively different properties when a few more vacancies are added. In contrast, two magnetic impurities in a metallic host may interact with each other, even indirectly, leading to a completely different ground-state, depending on the ratio of the relevant parameters [10, 11]. The phenomenology of the so-called two-impurity Anderson model [12] lies at the heart of the current understanding of important classes of compounds, such as heavy-fermions [13] and Kondo insulators [14].

Research on single-impurity systems received a large boost at the closing of last century with the observation of the Kondo effect in quantum dots (QDs) [15] and magnetic impurities on metal surfaces [16]. The ability to continuously tune the relevant Kondo-parameters in lithographically defined QDs opened the doors to detailed studies of the Kondo effect [17]. Subsequently, systems with two QDs were built [18] and, a few years later, indirect coupling between two QDs was being analyzed [19, 20]. In addition, in systems where there is competition between Kondo screening and other many-body interactions, a quantum phase transition (QPT) may occur, including the existence of non-Fermi liquid phases [21, 22]. This behavior may be experimentally studied in multi-QD systems [23, 24], in a single QD where there is orbital degeneracy [25], in single-molecule junctions [26, 27], and, more recently, in coupled hybrid metal–semiconductor islands [28].

In this work, we are interested in revisiting, using the numerical renormalization group (NRG) method [8, 9, 29], one specific double-QD (DQD) arrangement [see Fig. 1(a)], where only one of the QDs (QD₀) is connected to the leads, while the other (QD₁) is side-connected to QD₀, forming a T-shape or hanging dot geometry. This system has been shown to exhibit the well-known two-stage Kondo (TSK) effect [23, 24, 27, 30–42], which may happen in a variety of systems where there is more than one localized magnetic moment involved, thus creating an interplay between local and itinerant couplings [30, 31].

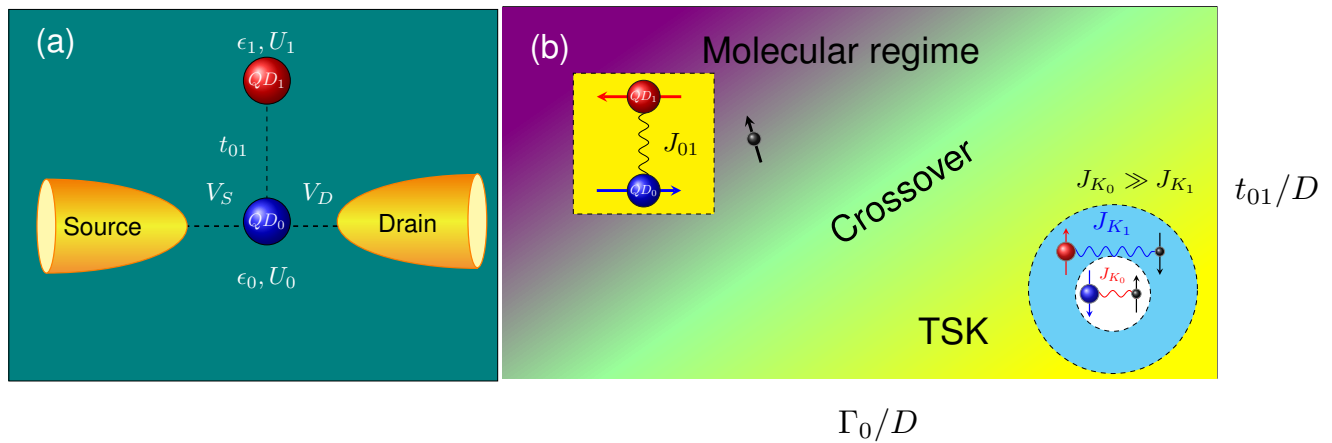


FIG. 1. (a) Schematic diagram of the DQD system in T-shape geometry. Only QD₀ is coupled to the source and drain leads through hoppings V_D and V_S . QD₀ and QD₁ are coupled by a hopping parameter t_{01} and their local energies are given by ϵ_0 and ϵ_1 , respectively. The on-site QD Coulomb interactions are U_0 and U_1 , where we take $U_0 = U_1 = U$, and we work in the PHS point, i.e., $\epsilon_0 = \epsilon_1 = -U/2$. (b) A schematic representation, in the $t_{01} - \Gamma_0$ parameter space, of the two regimes present in the DQD T-shape geometry system: right lower corner depicts the TSK regime, while the left upper corner contains the molecular regime (see text). The crossover region between these two regimes presents interesting effects resulting from competing interactions between the molecular regime, characterized by $J_{01} \approx 4t_{01}^2/U$, and the Kondo couplings J_{K_1} and J_{K_0} , which control the TSK regime.

For the DQD system with T-shape geometry [see Fig. 1(a)] in the TSK regime, QD₀ forms a Kondo state with the leads below a characteristic temperature T_{K_0} , while for $T < T_{K_1} \ll T_{K_0}$, QD₁ forms a Kondo state with the Fermi liquid resulting from the first-stage Kondo effect [32]. Our goal is to find an effective *single*-QD system that will reproduce QD₁'s Kondo physics (more specifically, its magnetic susceptibility and impurity spectral function) when QD₁ is in the second stage of the TSK effect. Based on the well-known universality of the Kondo effect, one expects that the Kondo physics of QD₁ should be *identical* to that of an effective *single* impurity Anderson model over a well-defined region of the $t_{01} - \Gamma_0$ parameter space with $U_{\text{eff}} = U_1$, $\epsilon_{\text{eff}} = \epsilon_1$, and with effective hybridization Γ_{eff} that is a function of t_{01} and Γ_0 . How well this effective model reproduces the Kondo properties of QD₁ can then be used to establish the range of values of t_{01} and Γ_0 where the DQD system is indeed in a TSK regime. We will see that this approach is very useful in defining that range, and that, in reality, it is found to be quite restricted.

As depicted in Fig. 1(b), the main result obtained in this work is the determination of a region in the $t_{01} - \Gamma_0$ parameter space where a *true* TSK regime occurs. This regime, located in the lower right-corner of Fig. 1(b), lies below a critical ratio t_{01}/Γ_0 , where the dominance of the coupling to the leads over the interdot coupling allows the sequential Kondo effects to occur. In this regime, the dominant interactions are the Kondo

interactions J_{K_0} and J_{K_1} [5], with $J_{K_0} \gg J_{K_1}$. On the opposite corner, in Fig. 1(b), lies the molecular regime, where the ratio t_{01}/Γ_0 is such that $J_{01} \approx 4t_{01}^2/U$ dominates, locking the QDs into a singlet, effectively disconnecting the DQD spins from the Fermi sea. The TSK and molecular regimes are separated by a crossover region, where these interactions compete. Finding the effective model that defines the TSK region may help design T-shape experimental setups to precisely tune the system into this region, and from there move into the crossover region and explore its properties.

This paper is organized as follows. In Sec. II, we present the model used and the associated Hamiltonian, followed by the NRG results in Sec. III, which is divided into several subsections. First, in subsection III A, we define the susceptibility for QD₁, then we introduce a SIAM effective model in subsection III B, which is further analyzed in subsection III C. The effective model is then used to study the spectral function of QD₁ in subsection III D, followed by two subsections analyzing the inter-QD spin correlations, subsections III E and III F. Finally, in subsection III G we analyze the universality of the inter-QD spin correlations. Section IV presents a summary and our conclusions.

II. Model and Hamiltonian

In Fig. 1(a), we show the system being analyzed in this work. Quantum dot QD₀ is connected to source and drain leads through hoppings V_S and V_D , respectively, while QD₁ is coupled only to QD₀ through a hopping t_{01} . We model this system through a double-impurity Anderson model, whose Hamiltonian is given by $H = H_{\text{DQD}} + H_{\text{leads}} + H_{\text{hyb}}$, where

* pa819824@ohio.edu

† ulloa@ohio.edu

‡ gbmartins@ufu.br

the first term (H_{DQD}), describing the DQD, is

$$H_{\text{DQD}} = \sum_{i\sigma} \epsilon_i n_{i\sigma} + \sum_i U_i n_{i\uparrow} n_{i\downarrow} - t_{01} \sum_{\sigma} (d_{0\sigma}^\dagger d_{1\sigma} + \text{H.c.}), \quad (1)$$

where $i = 0, 1$ labels the QDs, $n_{i\sigma} = d_{i\sigma}^\dagger d_{i\sigma}$ is the number operator for QD $_i$, thus $d_{i\sigma}$ annihilates an electron with spin $\sigma = \uparrow, \downarrow$ in QD $_i$, while U_i is the Coulomb repulsion in QD $_i$ and ϵ_i is its orbital energy. Finally, t_{01} is the amplitude for interdot hopping. The second term (H_{leads}), describing the source ($r = S$) and drain ($r = D$) leads, is given by

$$H_{\text{leads}} = \sum_{\vec{k}\sigma r} \epsilon_{r\vec{k}\sigma} n_{r\vec{k}\sigma}, \quad (2)$$

where $n_{r\vec{k}\sigma} = c_{r\vec{k}\sigma}^\dagger c_{r\vec{k}\sigma}$ is the number operator for a state with energy $\epsilon_{r\vec{k}\sigma}$ in lead r . The third term, containing the coupling between QD $_0$ and the leads, is given by

$$H_{\text{hyb}} = \sum_{\vec{k}\sigma r} (V_{r\vec{k}\sigma} d_{0\sigma}^\dagger c_{r\vec{k}\sigma} + \text{H.c.}), \quad (3)$$

where $V_{r\vec{k}\sigma}$ is the (spin conserving) hopping from QD $_0$ to lead $r = S, D$. Taking $V_{S\vec{k}\sigma} = V_{D\vec{k}\sigma} = V_0$, QD $_0$ couples only to the symmetric combination of both leads, through hopping $V = \sqrt{2}V_0$; then the hybridization between QD $_0$ and the band is given by $\Gamma_0 = \pi V^2 \rho_0$, where ρ_0 is the lead density of states (DOS) at the Fermi energy. For simplicity, we chose to take $V_S = V_D$, since, as is well known in Kondo physics, this simplifies the problem, without introducing any spurious effects [5]. We also consider the metallic host as having a uniform (flat) DOS in the interval $-D \leq \omega \leq D$, where $D = 1$, half of the bandwidth, is the energy unit. In addition, for simplicity, we consider $U_0 = U_1 = U$ and $\epsilon_0 = \epsilon_1 = -U/2$, i.e., that the system is in the particle-hole symmetric (PHS) point. The NRG calculations were done using the NRG Ljubljana code [43]. For most of the calculations, we have used the discretization parameter $\Lambda = 2.0$ and kept at least 5000 states at each iteration. We also employ the z-trick [44] (with $z = 0.25, 0.5, 0.75$, and 1.0 , i.e., $N_z = 4$) to remove oscillations (artifacts) in the physical quantities (for examples of its use, see Ref. [45]). The thermodynamic quantities were calculated using the traditional single-shell approximation, while the dynamical quantities (spectral function) were calculated using the density matrix NRG approximation [46].

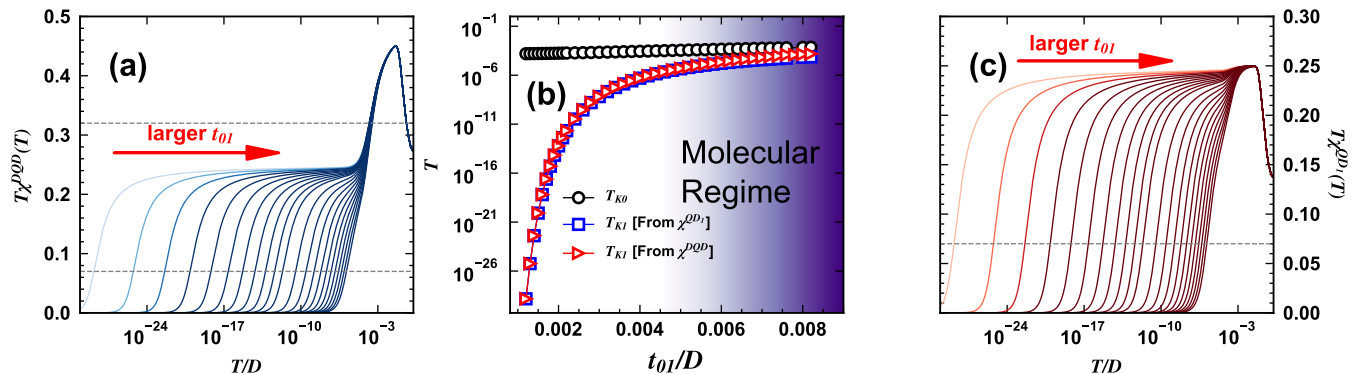


FIG. 2. (a) $T \chi^{DQD}(T)$ vs T for $U = 0.5$, $\Gamma_0 = 0.035$ and $0.0012 \leq t_{01} \leq 0.0022$ in steps of 0.0001 , and for $0.0024 \leq t_{01} \leq 0.0044$ in steps of 0.0002 . The red arrow indicates increasing t_{01} values. (b) Variation of both Kondo temperatures with t_{01} , T_{K_0} (black circles) and T_{K_1} (blue squares and red triangles), for the same Γ_0 as in (a). As expected, T_{K_0} is very weakly dependent on t_{01} , while T_{K_1} varies by ≈ 20 orders of magnitude and takes extremely low values for the smaller t_{01} values. The different ways of obtaining T_{K_1} are discussed in the text. The shading on the right side of the panel is to indicate the region where the system is increasingly in a molecular regime, and no longer in a TSK regime. (c) $T \chi^{DQD}(T)$ vs T for the same parameters as in panel (a). The red arrow has the same meaning as in panel (a). The horizontal gray dashed lines in panels (a) and (c) indicate the values of the Wilson criterion parameter α_i discussed in the text.

III. NRG Results

A. Obtaining T_{K_1} in two different ways: defining the magnetic susceptibility for QD $_1$

We use the Wilson criterion [5] for obtaining T_{K_0} and T_{K_1} , viz., $T_{K_i} \chi^{DQD}(T_{K_i}) = \alpha_i$, where $\alpha_0 = 0.25 + 0.07 = 0.32$ and $\alpha_1 = 0.07$. Here, χ^{DQD} is the DQD contribution to the total susceptibility, and it is obtained by calculating the total

system susceptibility (including the leads) and subtracting the susceptibility of a reference system, i.e., the system *without* the DQD (i.e., the Fermi sea or ‘bath’—see discussion around Eq. (47) in Ref. [29]). Figure 2(a) shows $T \chi^{DQD}(T)$ as a function of temperature, for $\Gamma_0 = 0.035$, in the interdot coupling range $0.0012 \leq t_{01} \leq 0.0044$. The two horizontal dashed lines indicate the α_i values mentioned above, used to obtain T_{K_i} . Figure 2(b) shows T_{K_0} (black circles) and T_{K_1} (red triangles), as a function of t_{01} , obtained as in Fig. 2(a), but now for t_{01} up

to 0.0082, i.e., very much inside the molecular regime. The results in panel (b) show that, as t_{01} decreases, T_{K_0} remains almost constant (as expected, since it should depend much more strongly on Γ_0 than on t_{01}), while T_{K_1} decreases by several orders of magnitude. As it will become clearer below, for a fixed value of Γ_0 there is a t_{01} value above which the system crosses into the molecular regime, and there is no more Kondo screening and the quantities T_{K_0} and T_{K_1} cease to be meaningful. The shading in Fig. 2(b) is meant to depict the molecular regime (see Ref. [32]).

By choosing a different reference system, we may calculate the contribution of *just* QD₁ to the susceptibility. Indeed, by subtracting, from the total system susceptibility, the susceptibility of the Fermi sea *plus* QD₀ (coupled to the Fermi sea by Γ_0), we obtain χ^{QD_1} , the QD₁ susceptibility. For the same parameters as in Fig. 2(a), $T\chi^{QD_1}(T)$ is shown in Fig. 2(c). Applying the Wilson criterion, with $\alpha_1 = 0.07$ [horizontal dashed line in panel (c)], to $T\chi^{QD_1}$, we obtain the blue squares in panel (b). The excellent agreement between the two methods [compare blue squares and red triangles in Fig. 2(b)] confirms that the definition of the susceptibility of QD₁ is sound. It is the susceptibility of QD₁, χ^{QD_1} , that will be used to assess the validity of a *single* impurity Anderson model, here dubbed an *effective model*, as described in the next section.

B. The effective model: fixed Γ_0 and varying t_{01}

Based on the universality of the Kondo effect, we expect that the Kondo physics of QD₁ should be, at least in some region of the $t_{01} - \Gamma_0$ parameter space, *identical* to that of an effective SIAM with $U_{\text{eff}} = U_1$, $\epsilon_{\text{eff}} = \epsilon_1 = -U/2$, and with an effective hybridization Γ_{eff} that should depend on t_{01} and Γ_0 . Indeed, Fig. 3(a) shows the fitting (black dashed curves) of $T\chi^{QD_1}$ (solid color curves) for the interval $0.0012 \leq t_{01} \leq 0.0038$. By appropriately adjusting the value of Γ_{eff} (which functions as a fitting parameter), for each different value of t_{01} (for $\Gamma_0 = 0.035$), we are able to accurately reproduce the $T\chi^{QD_1}$ results (color curves) in Fig. 3(a) over a range of t_{01} values. This is shown by the dashed black curves in Fig. 3(a), which faithfully reproduce the $T\chi^{QD_1}$ up to temperatures several orders of magnitude higher than T_{K_1} [47]. As t_{01} increases [panels (b) to (d)], the fitting is accurate only up to lower and lower temperatures, since the system is crossing over to the molecular regime, where the QDs form a *local* singlet among themselves, and not even the first Kondo stage occurs. It is interesting to contrast what happens in panel (a) (TSK regime), around the local moment (LM) fixed point, for QD₁ and the effective model [see the inset in panel (b)]: since QD₁ is not connected directly to the Fermi sea, it undergoes very small charge fluctuations, thus its susceptibility is very close to 1/4 for all t_{01} values (colored solid curves), while it decreases considerably as Γ_{eff} increases for the effective SIAM (black dashed curves).

Figure 4 presents the Γ_{eff} values as a function of t_{01} . It is interesting to see that the region for smaller values of t_{01} where one expects the TSK to occur [32], presents an almost linear dependence of Γ_{eff} with t_{01} .

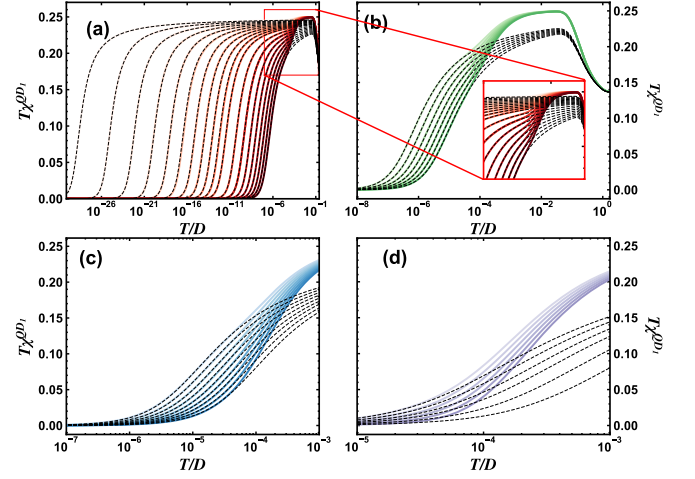


FIG. 3. $T\chi^{QD_1}$ vs. T results (colored solid curves) compared to the results obtained through an effective SIAM (black dashed curves) for different values of t_{01} . Parameters are $U_0 = U_1 = 0.5$, $\epsilon_0 = \epsilon_1 = -U/2$, and $\Gamma_0 = 0.035$. (a) $0.0012 \leq t_{01} \leq 0.0022$ in steps of 0.0001 and $0.0024 \leq t_{01} \leq 0.0038$ in steps of 0.0002; (b) $0.0040 \leq t_{01} \leq 0.0052$ in steps of 0.0002; (c) $0.0054 \leq t_{01} \leq 0.0070$ in steps of 0.0002; (d) $0.0072 \leq t_{01} \leq 0.0082$ in steps of 0.0002. The inset in panel (b) is a zoom in of the data in panel (a) of the local moment fixed point temperature range. Panel (a) displays excellent agreement with the effective model in that t_{01} range, which dissipates for higher t_{01} in (b)-(d).

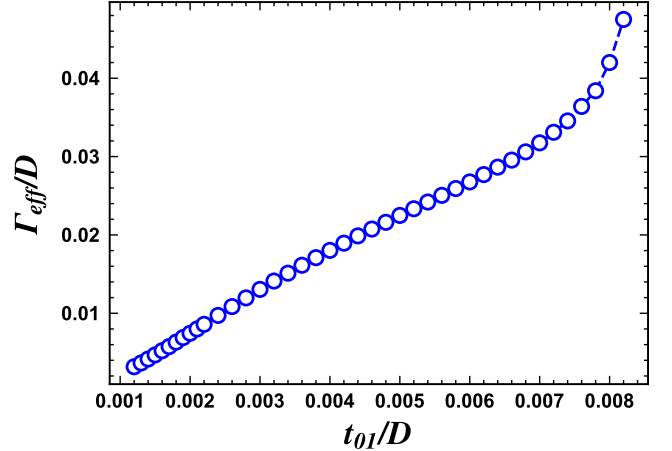


FIG. 4. Γ_{eff} vs t_{01} results (blue circles), as obtained through the fittings done in Fig. 3. Notice the initial near linear dependence of Γ_{eff} on t_{01} .

C. QD₁ susceptibility for fixed t_{01} and varying Γ_0

We now analyze χ^{QD_1} for varying coupling to the leads Γ_0 and a fixed t_{01} value. To help interpret these results, one should note that $T\chi$ (if we take a unit value for the gyromagnetic factor g , Bohr magneton μ_B , and Boltzmann constant k_B) measures S_z^2 , i.e., the square of the z -component of the magnetic impurity spin. Thus, χ^{DQD} measures $S_{DQD,z}^2$ and χ^{QD_1} measures $S_{1,z}^2$, where $\vec{S}_{DQD} = \vec{S}_0 + \vec{S}_1$. The left panel in Fig. 5

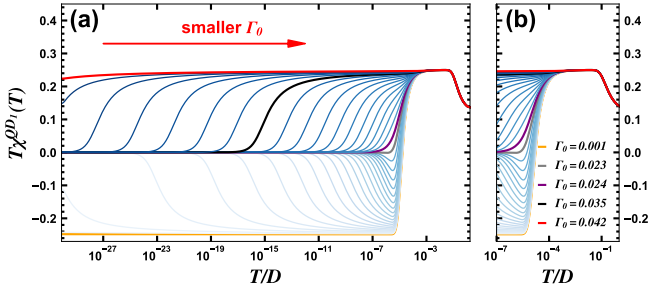


FIG. 5. (a) $T\chi^{QD1}$ vs T , for $0.002 \leq \Gamma_0 \leq 0.042$. The system is in the PSH point, $U = 0.5$, and $t_{01} = 0.0018$. The red arrow indicates the direction of decreasing Γ_0 . (b) Zoom in, around the LM temperature interval, of the data in panel (a). The legend applies to both panels.

shows $T\chi^{QD1}$ as a function of temperature, in the PHS point, for $0.002 \leq \Gamma_0 \leq 0.042$, $t_{01} = 0.0018$, and $U = 0.5$. The red curve is for $\Gamma_0 = 0.042$ (largest Γ_0 and lowest T_{K1}), where T_{K1} increases as Γ_0 decreases (the red arrow points in the direction of decreasing Γ_0 curves). The black curve is for $\Gamma_0 = 0.035$, resulting in $T_{K1} = 1.05 \times 10^{-15}$. Figure 5(b) shows a zoom of the LM fixed point temperature region. It is interesting to note that, for temperatures just below the LM temperature region (marked by the $S_{1,z}^2 = 1/4$ plateau), the QD₁ susceptibility for $\Gamma_0 = 0.023$ (gray curve) becomes slightly negative, before vanishing. For progressively smaller Γ_0 values, the susceptibility will dip into more and more negative values, before going through an upturn and then vanishing as $T \rightarrow 0$. For even smaller Γ_0 values, the dip approaches $-1/4$, forming a plateau at this value, eventually upturning and vanishing. This behavior reflects the procedure used to obtain χ^{QD1} as follows. For $0.001 \leq \Gamma_0 \leq 0.023$ (the smaller Γ_0 values) and $t_{01} = 0.0018$, the system is in the molecular regime (as will be shown in Fig. 11). There, for temperatures just below the LM fixed point, the DQD system has $S_{DQD,z}^2 \approx 0$, because of the inter-QD singlet formation (see Fig. 6). However, since we subtract the susceptibility of QD₀ (our reference in the χ^{QD1} calculation), which, for this temperature and Γ_0 interval, is of the order of $S_{0,z}^2 \lesssim 1/4$, the result for $T\chi^{QD1}$ must become negative and then (as Γ_0 decreases) form a plateau at $\approx -1/4$. For temperatures below T_{K0} , when $S_{0,z}^2$ (the reference) vanishes (due to Kondo), then $S_{1,z}^2 - S_{0,z}^2$ also vanishes (since both are ≈ 0). Thus, this calculation of the susceptibility for QD₁ for the smaller Γ_0 values is revealing. It is able to clearly spot the molecular regime (the onset of negative values for $T\chi^{QD1}$), an effect that is not as apparent when we analyze $T\chi^{DQD}$ (Fig. 6). Note that the results in Fig. 5 indicate that, for $\Gamma_0 \approx 0.023$ (and $t_{01} = 0.0018$) the system is in the final stage of the crossover into the molecular regime.

Figure 6 presents results for $T\chi^{DQD}$, as a function of temperature, for the same parameters as in Fig. 5. It is interesting to note that there is one specific temperature at which the susceptibility is the same ($T\chi^{DQD} \approx 1/4$) for all Γ_0 , indicated by a blue arrow. This energy scale is of the same order of magnitude as that signaling the crossover into the molecular regime, $\approx 10^{-5}$. We redid the calculations in Fig. 6 for different t_{01} values, and obtained that the crossing still occurs at $T\chi^{DQD} \approx 1/4$,

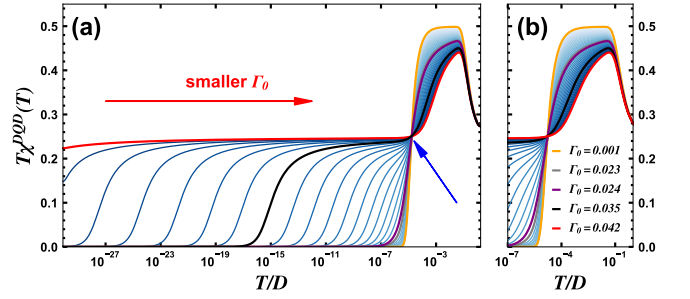


FIG. 6. (a) $T\chi^{DQD}$ vs T for several Γ_0 values. Same parameters and same colors as in Fig. 5. The red arrow points in the direction of decreasing Γ_0 curves. The blue arrow points to the peculiar crossing of all curves in a single point. (b) Zoom in, around the LM temperature interval, of the data in panel (a). The legend applies to both panels.

albeit at slightly different temperatures, while the crossing has no dependence on ϵ_d .

D. QD₁ spectral function and the effective SIAM

As shown in the previous two subsections, the effective model provides an excellent description of the magnetic susceptibility of QD₁, yields a good understanding of the physics around the LM fixed point [see inset in Fig. 3(b)], and affords a quantitative way of determining when the system enters the molecular regime. Then, one may ask whether the effective model can describe the dynamic properties of QD₁. Figure 7 shows the spectral functions $A_0(\omega)$ and $A_1(\omega)$, for QD₀ and QD₁, in panels (a) and (b), respectively. The spectral functions were calculated using the density matrix NRG approximation [46]. It is well known [32] that an antiresonance appears at the Fermi energy in $A_0(\omega)$, with a characteristic width T_{K1} . This has been well studied in the literature and it is shown in the inset to Fig. 7(a). However, $A_1(\omega)$ has received much less attention [40]. Its peculiar shape [blue curve in Fig. 7(b)], with a Kondo peak much shorter than the Coulomb blockade peaks, has its origin in the fact that the Friedel Sum Rule for the DQD system has a much different expression from the well-known one for the SIAM [5], as illustrated in the case of a two-level QD system [48], for example. Because of that, it is clear that $A_{\text{eff}}(\omega)$ will not simulate $A_1(\omega)$ for an ω -range that includes the Coulomb blockade peaks.

Thus, as shown in Fig. 8, we limit the comparison of the spectral functions to an ω -range around the Fermi energy that excludes the Hubbard peak. We normalize to 1 the height of both Kondo peaks, the one obtained from the effective model (black dashed curves) [49] and the one from the DQD (colored solid curves), to facilitate comparison. It is important to stress that no further adjustments are needed to the effective model. In other words, the values of Γ_{eff} used to obtain $A_{\text{eff}}(\omega)$ are the ones obtained from the susceptibility fittings in Fig. 3, and shown explicitly in Fig. 4 [50]. The spectral function comparisons are shown in Fig. 8, for $\Gamma_0 = 0.035$ and t_{01} in the interval $0.0012 \leq t_{01} \leq 0.0024$, as indicated in the legend. The agreement between $A_1(\omega)$ (colored solid

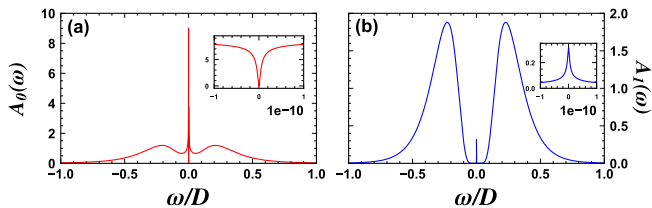


FIG. 7. (a) QD₀ spectral function $A_0(\omega)$ for $\Gamma_0 = 0.035$, $U = 0.5$, and $t_{01} = 0.0022$, in the PHS point. The inset shows the antiresonance ‘inside’ the Kondo peak. (b) QD₁ spectral function $A_1(\omega)$ for the same parameters as in (a). The inset shows a zoom of the very small Kondo peak in QD₁. The spectral functions in both panels integrate to unity.

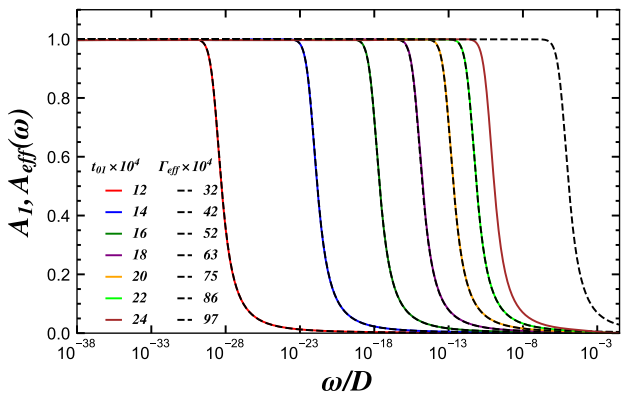


FIG. 8. Comparison between the spectral functions $A_1(\omega)$ (colored solid curves) and $A_{\text{eff}}(\omega)$ (dashed black curves) in the range $10^{-38} \leq \omega/D \leq 10^{-2}$ for several values of t_{01} (as indicated in the legend). Parameters used are $0.0012 \leq t_{01} \leq 0.0024$, $U = 0.5$, $\Gamma_0 = 0.035$, and the system is in the PHS point. The corresponding values of Γ_{eff} are indicated. Note that for $t_{01} = 0.0024$ there is no agreement between $A_1(\omega)$ (solid curve) and $A_{\text{eff}}(\omega)$ (dashed curve).

curves) and $A_{\text{eff}}(\omega)$ (black dashed curves), up to $t_{01} = 0.0022$ is remarkable. For $t_{01} \geq 0.0024$, the Kondo peaks for QD₁ and the effective model deviate from each other (as shown for $t_{01} = 0.0024$). These results suggest a different criterion to determine the range of t_{01} values where the second Kondo effect can be truly simulated by the SIAM. The spectral function comparisons indicate that the upper limit for t_{01} is considerably smaller than what transpires from the $T\chi^{QD_1}$ fittings in Fig. 3(a), and what has been often determined in the literature as the TSK-regime range [32].

In the next subsections, we will study some aspects of the inter-QD spin correlation $\langle \vec{S}_0 \cdot \vec{S}_1 \rangle$ and show that its variation with the system parameters (Γ_0 and t_{01}) may be used to further characterize the TSK regime.

E. Inter-QD spin correlations: Dependence on t_{01}

Figure 9 presents $\langle \vec{S}_0 \cdot \vec{S}_1 \rangle$ for $0.0012 \leq t_{01} \leq 0.0082$, $\Gamma_0 = 0.035$, $U = 0.5$, $T \approx 10^{-27}$ (ground state), for the system

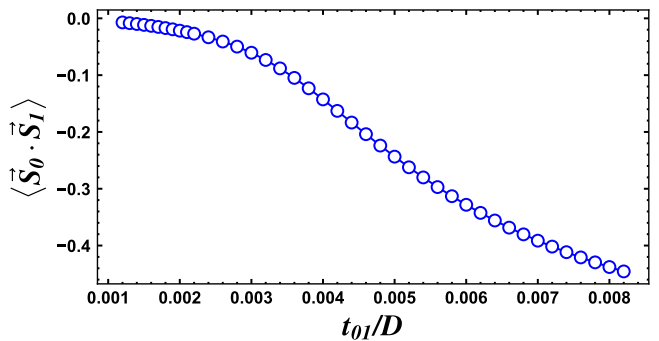


FIG. 9. Ground state ($T \approx 10^{-27}$) interdot spin correlations. $\langle \vec{S}_0 \cdot \vec{S}_1 \rangle$ vs t_{01} for $U = 0.5$, $\Gamma_0 = 0.035$, with the system in the PHS point.

in the PHS point. Three different regions may be discerned. For very small t_{01} values, when the system is in the TSK regime and thus each QD is ‘locked’ into its own Kondo state, there is very little correlation between the QDs. On the other hand, for the largest t_{01} values (molecular regime), the first Kondo stage does not occur (thus, neither the second), since the two QDs are strongly antiferromagnetically linked by its correlation, which tends to the full singlet value of $-3/4$. Then, in an intermediate region of t_{01} values, there is a crossover between the TSK and the molecular regimes.

It is interesting to study $\langle \vec{S}_0 \cdot \vec{S}_1 \rangle$ as a function of temperature in the interval $0.0012 \leq t_{01} \leq 0.0036$, for $\Gamma_0 = 0.035$, $U = 0.5$, in the PHS point. This is shown in Fig. 10(a), also with values of T_{K_1} (yellow circles), T_{K_0} (green up-triangles), and $J_{01} = 4t_{01}^2/U$ (orange right-triangles, representing the effective antiferromagnetic (AF) coupling between the two QDs). The symbols for each of these three energy scales, which depend on t_{01} , are placed on top of the corresponding $\langle \vec{S}_0 \cdot \vec{S}_1 \rangle$ vs T curve. The red curve indicates $t_{01} = 0.0022$, which marks the end of the TSK regime, according to the spectral function analysis of the effective model. At high temperatures, the correlations vanish for all t_{01} values, as expected. As the temperature decreases, AF correlations between the QDs start to develop, and they are enhanced (becoming more negative) even for temperatures below T_{K_0} [marked by the green up-triangles, see zoom ins in panels (b) and (c)], indicating that QD₀ develops singlet correlations simultaneously with the conduction electrons (forming the Kondo singlet) and with QD₁, mainly when in the crossover regime ($t_{01} > 0.0022$). Indeed, inside the crossover regime, $0.0022 < t_{01} \leq 0.0036$, the singlet correlations between the two QDs are strongly enhanced, for temperatures below T_{K_0} , finally settling into a plateau. This can be seen as a precursor to the full molecular regime.

Now, let us analyze the onset of the second Kondo stage for the larger values of t_{01} . It is clear that down to $t_{01} \approx 0.003$ [fourth curve from bottom to top in panel (a)], T_{K_1} marks the temperature where the plateau in $\langle \vec{S}_0 \cdot \vec{S}_1 \rangle$ starts. In contrast, for the smallest values of t_{01} , as shown in panel (b), it is the energy scale J_{01} (orange right-triangles) that marks the onset of the $\langle \vec{S}_0 \cdot \vec{S}_1 \rangle$ plateau. For intermediate values of t_{01} , the

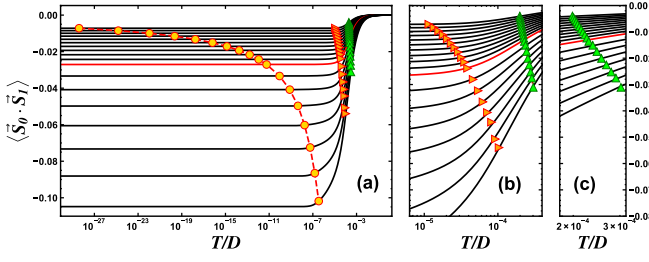


FIG. 10. (a) $\langle \vec{S}_0 \cdot \vec{S}_1 \rangle$ vs T for $0.0012 \leq t_{01} \leq 0.0022$, in steps of 0.0001, and for $0.0022 \leq t_{01} \leq 0.0036$, in steps of 0.0002. Parameters used are $U = 0.5$, $\Gamma_0 = 0.035$, and system in the PHS point. The red curve is for $t_{01} = 0.0022$. The yellow circles indicate T_{K_1} , the orange triangles $J_{01} = 4t_{01}^2/U$, and the green triangles T_{K_0} . (b) and (c) are progressive zoom ins on the data in panel (a) at higher temperatures.

plateau onset occurs for an energy scale that is intermediate between J_{01} and T_{K_1} . Note that this analysis, for $t_{01} > 0.0036$ (for $\Gamma_0 = 0.035$), becomes questionable, since the very use of the T_{K_0} and T_{K_1} energy scales loses its meaning.

One interesting aspect of the results in Fig. 10(a) is that for temperatures below T_{K_1} (yellow circles), there is virtually no change in $\langle \vec{S}_0 \cdot \vec{S}_1 \rangle$ as the QD₁ spin is screened by the conduction electrons via the formation of the second Kondo state. This is especially true inside the TSK regime, where the plateau starts at temperatures well above T_{K_1} . In other words, the formation of a correlated state between QD₁ and the conduction electrons (the second Kondo state) does not alter the spin correlation of QD₁ with QD₀.

F. Inter-QD spin correlations: Dependence on Γ_0

Figure 11 shows how $\langle \vec{S}_0 \cdot \vec{S}_1 \rangle$ varies with Γ_0 for three different t_{01} values, *viz.*, 0.0018, 0.0040, and 0.0082, for $T \approx 10^{-27}$ (ground state). For very small values of Γ_0 (up to ≈ 0.015) the QDs form a strong singlet ($\langle \vec{S}_0 \cdot \vec{S}_1 \rangle \approx -0.75$, indicated by the solid gray horizontal line), independent of the value of t_{01} . Thus, all three t_{01} values place the system in the molecular regime for such small Γ_0 values. Larger Γ_0 values ($\Gamma_0 \geq 0.025$), show a clear separation between the three curves: for the lowest $t_{01} = 0.0018$ (red circles), $\langle \vec{S}_0 \cdot \vec{S}_1 \rangle$ rapidly vanishes with increasing Γ_0 , while for $t_{01} = 0.0040$ (green squares), $\langle \vec{S}_0 \cdot \vec{S}_1 \rangle$ is still strongly AF, but approaches zero as Γ_0 increases, as it will eventually crossover into the TSK regime. The $\langle \vec{S}_0 \cdot \vec{S}_1 \rangle$ results for $t_{01} = 0.0082$ (blue triangles), however, display sizeable AF values for nearly the whole Γ_0 interval in Fig. 11, have a markedly different dependence on Γ_0 , and become negligible only for Γ_0 values large enough to place QD₀ close to (or into) an intermediate valence regime [5].

Coming back to the $t_{01} = 0.0018$ results (red circles), the spectral function in Fig 8(d) shows that for $\Gamma_0 = 0.035$ the system is well into the TSK regime, since the QD₁ dynamical properties agree with the SIAM effective model. Obviously, larger values of Γ_0 will maintain the system in the TSK

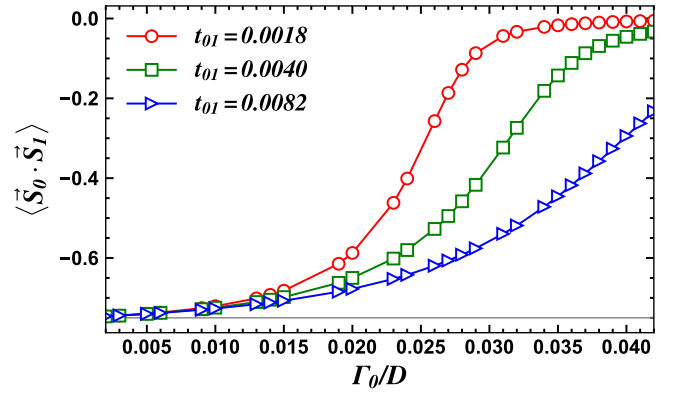


FIG. 11. Ground state $\langle \vec{S}_0 \cdot \vec{S}_1 \rangle$ vs. Γ_0 for $t_{01} = 0.0018$ (red circles), $t_{01} = 0.0040$ (green squares), and $t_{01} = 0.0082$ (blue triangles) for $0.002 \leq \Gamma_0 \leq 0.042$, $U = 0.5$, and system in the PHS point. The horizontal light-gray line indicates the full-singlet value $\langle \vec{S}_0 \cdot \vec{S}_1 \rangle = -3/4$.

regime. The functional form of the red circles curve in Fig. 11 seems related to that of the other two curves, which motivates one to explore re-scaling properties. This probing for universal behavior is carried out in the next subsection.

G. Collapse of the inter-QD spin correlations

Figure 12(a) shows the $\langle \vec{S}_0 \cdot \vec{S}_1 \rangle$ vs Γ_0 curves in the interval $0.0012 \leq t_{01} \leq 0.0082$. In accordance to the discussion above, we use the lowest $t_{01} = 0.0012$ curve in Fig. 12(a) as the ‘target’ curve, and try to collapse higher t_{01} -value curves onto it. We apply the following procedure. First, we choose a ‘reference’ value, denoted Γ_0^{ref} , inside the TSK region of the target curve. Next, we find what is the Γ_0 value (denoted $\Gamma_0^{0.0012}$) for which $\langle \vec{S}_0 \cdot \vec{S}_1 \rangle(t_{01} = 0.0012, \Gamma_0^{0.0012}) = \langle \vec{S}_0 \cdot \vec{S}_1 \rangle(t_{01}, \Gamma_0^{\text{ref}})$, providing the re-scaling factor by which we divide the Γ_0 axis for the t_{01} curve in question, $\xi = \Gamma_0^{\text{ref}}/\Gamma_0^{0.0012}$. Panel (b) shows the re-scaled results in the interval $0.0013 \leq t_{01} \leq 0.0023$, using $\Gamma_0^{\text{ref}} = 0.027$, where all curves collapse onto the curve for $t_{01} = 0.0012$ (black solid curve). Panel (c) shows that applying the same re-scaling procedure for $t_{01} > 0.0023$ curves does not produce as good a collapse onto the target curve.

It should be noted that the $\langle \vec{S}_0 \cdot \vec{S}_1 \rangle$ curves for larger values of t_{01} [see panel (c)] may re-scale for larger values of Γ_0^{ref} , at least until a certain value of t_{01} . This reflects the fact that it is the ratio t_{01}/Γ_0 that determines if the system is in the TSK regime or not (as long as Γ_0 does not result in a mixed valence regime).

Figure 13 shows $\langle \vec{S}_0 \cdot \vec{S}_1 \rangle$ as a color map in the $t_{01} - \Gamma_0$ parameter space. We can use it to delineate a region where the TSK regime resides. For that, we use the spectral function results obtained previously, where we found the maximum $t_{01} = 0.0022$ (for $\Gamma_0 = 0.035$) for which the QD₁ Kondo peak could be accurately simulated through the effective model. For these values we obtain $\langle \vec{S}_0 \cdot \vec{S}_1 \rangle(0.0022, 0.035) = -0.027$.

Taking that as the lower limit for $\langle \vec{S}_0 \cdot \vec{S}_1 \rangle$, that defines the border of the TSK regime, we obtain the slanted black line close to the lower right corner in Fig. 13. In other words, this is the

line where $\langle \vec{S}_0 \cdot \vec{S}_1 \rangle(t_{01}, \Gamma_0) = -0.027$ in the $t_{01} - \Gamma_0$ plane. The yellow region, for which $\langle \vec{S}_0 \cdot \vec{S}_1 \rangle(t_{01}, \Gamma_0) > -0.027$, defines the TSK regime.

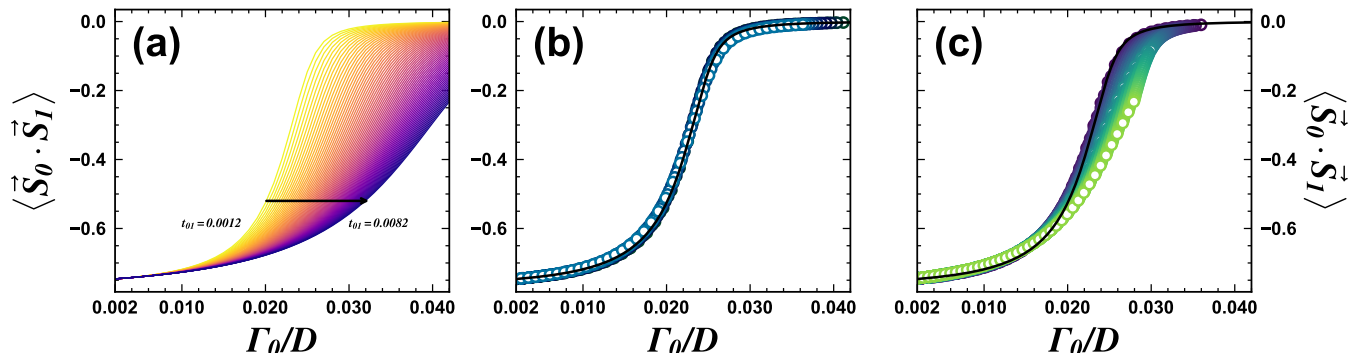


FIG. 12. (a) Ground state $\langle \vec{S}_0 \cdot \vec{S}_1 \rangle$ vs Γ_0 for $0.0012 \leq t_{01} \leq 0.0082$ (from left to right, see horizontal arrow). (b) Re-scaled $0.0012 \leq t_{01} \leq 0.0023$ results, showing their collapse onto the $t_{01} = 0.0012$ curve (black solid line). (c) $\langle \vec{S}_0 \cdot \vec{S}_1 \rangle$ results for the interval $0.0024 \leq t_{01} \leq 0.0082$, showing that these results do not share universality with the lower t_{01} results in panel (b).

IV. Summary and Conclusions

In summary, we have analyzed a T-shape geometry for a DQD system, using NRG. Our simulation through a two-impurity Anderson model is focused on determining the $t_{01} - \Gamma_0$ parameter region in which the second Kondo stage can be well defined. We were able to show, using an effective SIAM, that the TSK regime occupies a rather restricted sector of parameter space (see Fig. 13). The process of obtaining this result required the calculation of the QD_1 susceptibility, its comparison with the susceptibility of an effective SIAM, as well as the comparison of the dynamic properties of QD_1 . We found that in the region where the “better-defined” TSK occurs (for fixed Γ_0 and small values of t_{01}), Γ_{eff} depends linearly on t_{01} (see Fig. 4).

To supplement the information and perspective that χ^{QD_1} and $A_1(\omega)$ can provide, we also carried out a thorough analysis of the inter-QD spin correlations $\langle \vec{S}_0 \cdot \vec{S}_1 \rangle$. This allowed us to uncover interesting features of the DQD system, *viz.*, the TSK manifests itself through the appearance of a plateau in the interdot spin correlation for $T < J_{01}$ (see Fig. 10) and through the universality of the $\langle \vec{S}_0 \cdot \vec{S}_1 \rangle$ vs Γ_0 curves for small enough t_{01} values.

We anticipate that our results could guide the study of related DQD systems. For example, when the QDs are in a parallel geometry [51], with both QDs connected to the leads (in that case, QD_1 connects through Γ_1 to the Fermi sea, while in T-geometry $\Gamma_1 = 0$). In that system, there is the possibility of a singlet/triplet QPT [40, 52, 53] through variation of the coupling parameters. For instance, when increasing Γ_1 (for fixed Γ_0 and t_{01}), the system eventually goes through a singlet/triplet QPT (as shown in Fig. 7(a) in Ref. [40]) [54]. It would be important to distinguish what is the character of the

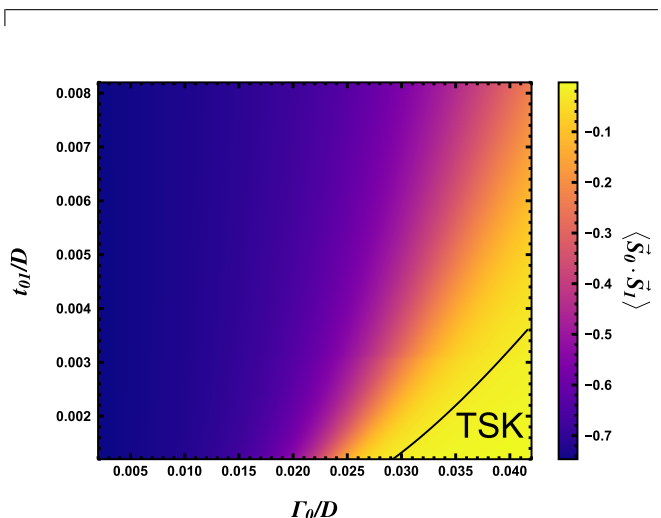


FIG. 13. $\langle \vec{S}_0 \cdot \vec{S}_1 \rangle$ color map in the $t_{01} - \Gamma_0$ parameter space. The solid line is defined as $\langle \vec{S}_0 \cdot \vec{S}_1 \rangle(t_{01}, \Gamma_0) = -0.027$ and delimits the location of the TSK regime, as defined in this work.

singlet-side of the QPT, *viz.*, the TSK, the molecular, or the crossover between them. Our results may provide guidance to experimentalists to better place the system in the desired regime.

Thus, we trust that our analysis allows experimental groups to tune the parameters of a DQD system with T-shape geometry into the *true* TSK regime. Varying parameters accordingly, they could study the crossover to the molecular regime, and turn on Γ_1 to study the singlet/triplet QPT starting from different singlet regimes.

Acknowledgments

We thank R. Žitko for helping with certain details of the use of the NRG Ljubljana package. P.A.A., S.E.U. and G.B.M. acknowledge support from the CAPES-PrInt/UFU program. P.A.A. thanks the Brazilian funding agency CAPES for financial support. E.V. acknowledges financial support from the

National Council for Scientific and Technological Development (CNPq), Grant No. 311366/2021-0. S.E.U. acknowledges support from the US Department of Energy, Office of Basic Energy Sciences, Materials Science and Engineering Division. E.V.A. acknowledges financial support from the National Council for Scientific and Technological Development (CNPq), Grant No. 307644/2022-7.

-
- [1] N. W. Ashcroft and N. D. Mermin, *Solid State Physics* (Holt-Saunders, 1976).
- [2] W. de Haas, J. de Boer, and G. van den Berg, The electrical resistance of gold, copper and lead at low temperatures, *Physica* **1**, 1115 (1934).
- [3] L. Hoddeson, E. Braun, J. Teichmann, and S. Weart, eds., *Out of the Crystal Maze: Chapters from The History of Solid State Physics* (Oxford University Press, United Kingdom, 1992).
- [4] J. Kondo, Resistance minimum in dilute magnetic alloys, *Prog. Theor. Exp. Phys.* **32**, 37 (1964).
- [5] A. C. Hewson, *The Kondo Problem to Heavy Fermions*, Cambridge Studies in Magnetism (Cambridge University Press, 1993).
- [6] P. W. Anderson, Localized magnetic states in metals, *Phys. Rev.* **124**, 41 (1961).
- [7] J. R. Schrieffer and P. A. Wolff, Relation between the Anderson and Kondo Hamiltonians, *Phys. Rev.* **149**, 491 (1966).
- [8] K. G. Wilson, The renormalization group: Critical phenomena and the Kondo problem, *Rev. Mod. Phys.* **47**, 773 (1975).
- [9] H. R. Krishna-murthy, J. W. Wilkins, and K. G. Wilson, Renormalization-group approach to the Anderson model of dilute magnetic alloys. I. Static properties for the symmetric case, *Phys. Rev. B* **21**, 1003 (1980).
- [10] B. A. Jones, C. M. Varma, and J. W. Wilkins, Low-temperature properties of the two-impurity Kondo Hamiltonian, *Phys. Rev. Lett.* **61**, 125 (1988).
- [11] B. A. Jones and C. M. Varma, Critical point in the solution of the two magnetic impurity problem, *Phys. Rev. B* **40**, 324 (1989).
- [12] O. Sakai, Y. Shimizu, and T. Kasuya, Excitation-spectra of 2 impurity Anderson model, *Solid State Commun.* **75**, 81 (1990); O. Sakai and Y. Shimizu, Excitation-spectra of 2 impurity Anderson model. 1. Critical transition in the 2 magnetic impurity problem and the roles of the parity splitting, *J. Phys. Soc. Jpn.* **61**, 2333 (1992); Excitation-spectra of 2 impurity Anderson model. 2. Interplay between the Kondo effect and the inter site interactions, *J. Phys. Soc. Jpn.* **61**, 2348 (1992).
- [13] G. R. Stewart, Heavy-fermion systems, *Rev. Mod. Phys.* **56**, 755 (1984).
- [14] H. Tsunetsugu, M. Sigrist, and K. Ueda, The ground-state phase diagram of the one-dimensional Kondo lattice model, *Rev. Mod. Phys.* **69**, 809 (1997).
- [15] D. Goldhaber-Gordon, H. Shtrikman, D. Mahalu, D. Abusch-Magder, U. Meirav, and M. Kastner, Kondo effect in a single-electron transistor, *Nature* **391**, 156 (1998).
- [16] L. Kouwenhoven and L. Glazman, Revival of the Kondo effect, *Phys. World* **14**, 33 (2001).
- [17] M. Pustilnik and L. Glazman, Kondo effect in quantum dots, *J. Phys. Condens. Matter* **16**, R513 (2004).
- [18] T. Oosterkamp, T. Fujisawa, W. van der Wiel, K. Ishibashi, R. Hijman, S. Tarucha, and L. Kouwenhoven, Microwave spectroscopy of a quantum-dot molecule, *Nature* **395**, 873 (1998).
- [19] N. Craig, J. Taylor, E. Lester, C. Marcus, M. Hanson, and A. Gossard, Tunable nonlocal spin control in a coupled-quantum dot system, *Science* **304**, 565 (2004).
- [20] G. B. Martins, C. A. Büsser, K. A. Al-Hassanieh, E. V. Anda, A. Moreo, and E. Dagotto, Transport properties of strongly correlated electrons in quantum dots studied with a simple circuit model, *Phys. Rev. Lett.* **96**, 066802 (2006).
- [21] R. Bulla and M. Vojta, Quantum phase transitions in models of magnetic impurities, in *Concepts in Electron Correlation*, edited by A. C. Hewson and V. Zlatić (Springer Dordrecht, 2003) Chap. 9, p. 209.
- [22] M. Vojta, Impurity quantum phase transitions, *Philos. Mag.* **86**, 1807 (2006).
- [23] S. Sasaki, H. Tamura, T. Akazaki, and T. Fujisawa, Fano-Kondo interplay in a side-coupled double quantum dot, *Phys. Rev. Lett.* **103**, 266806 (2009).
- [24] R. Žitko, Fano-Kondo effect in side-coupled double quantum dots at finite temperatures and the importance of two-stage Kondo screening, *Phys. Rev. B* **81**, 115316 (2010).
- [25] G. Zaránd, Orbital fluctuations and strong correlations in quantum dots, *Philos. Mag.* **86**, 2043 (2006).
- [26] F. Evers, R. Korytár, S. Tewari, and J. M. van Ruitenbeek, Advances and challenges in single-molecule electron transport, *Rev. Mod. Phys.* **92**, 035001 (2020).
- [27] X. Guo, Q. Zhu, L. Zhou, W. Yu, W. Lu, and W. Liang, Evolution and universality of two-stage Kondo effect in single manganese phthalocyanine molecule transistors, *Nat. Commun.* **12**, 1566 (2021).
- [28] W. Pouse, L. Peeters, C. L. Hsueh, U. Gennser, A. Cavanna, M. A. Kastner, A. K. Mitchell, and D. Goldhaber-Gordon, Quantum simulation of an exotic quantum critical point in a two-site charge Kondo circuit, *Nat. Phys.* **19**, 492 (2023).
- [29] R. Bulla, T. A. Costi, and T. Pruschke, Numerical renormalization group method for quantum impurity systems, *Rev. Mod. Phys.* **80**, 395 (2008).
- [30] W. Hofstetter and H. Schoeller, Quantum phase transition in a multilevel dot, *Phys. Rev. Lett.* **88**, 016803 (2001).
- [31] M. Vojta, R. Bulla, and W. Hofstetter, Quantum phase transitions in models of coupled magnetic impurities, *Phys. Rev. B* **65**, 140405(R) (2002).
- [32] P. S. Cornaglia and D. R. Gempel, Strongly correlated regimes in a double quantum dot device, *Phys. Rev. B* **71**, 075305 (2005).
- [33] R. Žitko and J. Bonča, Enhanced conductance through side-coupled double quantum dots, *Phys. Rev. B* **73**, 035332 (2006).
- [34] R. Žitko and J. Bonča, Correlation effects in side-coupled quantum dots, *J. Phys. Condens. Matter* **19**, 255205 (2007).
- [35] C.-H. Chung, G. Zarand, and P. Wölfle, Two-stage Kondo effect in side-coupled quantum dots: Renormalized perturbative scaling theory and numerical renormalization group analysis, *Phys.*

- Rev. B **77**, 035120 (2008).
- [36] H. Tamura and S. Sasaki, Fano-Kondo effect in side-coupled double quantum dot, *Physica E* **42**, 864 (2010).
- [37] I. L. Ferreira, P. A. Orellana, G. B. Martins, F. M. Souza, and E. Vernek, Capacitively coupled double quantum dot system in the Kondo regime, *Phys. Rev. B* **84**, 205320 (2011).
- [38] Y. Tanaka, N. Kawakami, and A. Oguri, Crossover between two different Kondo couplings in side-coupled double quantum dots, *Phys. Rev. B* **85**, 155314 (2012).
- [39] D. Y. Baines, T. Meunier, D. Maily, A. D. Wieck, C. Bäuerle, L. Saminadayar, P. S. Cornaglia, G. Usaj, C. A. Balseiro, and D. Feinberg, Transport through side-coupled double quantum dots: From weak to strong interdot coupling, *Phys. Rev. B* **85**, 195117 (2012).
- [40] Y.-H. Liao, J. Huang, and W.-Z. Wang, Real two-stage Kondo effect in parallel double quantum dot, *J. Magn. Magn. Mater.* **377**, 354 (2015).
- [41] M. Crisan, I. Grosu, and I. Tifrea, An equation of motion analysis of the two stage Kondo effect in T-shaped double-quantum-dot systems, *Physica E* **66**, 245 (2015).
- [42] X.-W. Chen, G.-Y. Yi, L.-L. Zhang, W.-B. Cui, and W.-J. Gong, Kondo physics in the T-shaped structure with two detuned quantum dots, *Physica E* **134**, 114928 (2021).
- [43] R. Žitko, *NRG Ljubljana* (2021).
- [44] V. L. Campo and L. N. Oliveira, Alternative discretization in the numerical renormalization-group method, *Phys. Rev. B* **72**, 104432 (2005).
- [45] P. A. Almeida, M. A. Manya, M. S. Figueira, S. E. Ulloa, E. V. Anda, and G. B. Martins, Quantum impurity with $2/3$ local moment in one-dimensional quantum wires: A numerical renormalization group study, *Phys. Rev. B* **109**, 045112 (2024).
- [46] W. Hofstetter, Generalized numerical renormalization group for dynamical quantities, *Phys. Rev. Lett.* **85**, 1508 (2000).
- [47] The Bethe-Ansatz could be an alternative to the NRG to calculate the effective model universal-susceptibility. See, for example, N. Andrei, K. Furuya, and J. H. Lowenstein, *Rev. Mod. Phys.* **55**, 331 (1983).
- [48] D. E. Logan, C. J. Wright, and M. R. Galpin, Correlated electron physics in two-level quantum dots: Phase transitions, transport, and experiment, *Phys. Rev. B* **80**, 125117 (2009).
- [49] Note that, as expected, $A_{\text{eff}}(\omega)$ obeys the Friedel Sum Rule, i.e., $\pi\Gamma_{\text{eff}}A_{\text{eff}}(0) = 1$.
- [50] As in the case of the possible use of the Bethe-Ansatz for the calculation of the effective model universal-susceptibility [47], here, we could alternatively use a universal expression for $A_{\text{eff}}(\omega)$, provided, for example, in H. O. Frota, *Phys. Rev. B* **45**, 1096 (1992).
- [51] R. Žitko and J. Bonča, Multiple-impurity Anderson model for quantum dots coupled in parallel, *Phys. Rev. B* **74**, 045312 (2006).
- [52] G. Zaránd, C.-H. Chung, P. Simon, and M. Vojta, Quantum criticality in a double-quantum-dot system, *Phys. Rev. Lett.* **97**, 166802 (2006).
- [53] R. Žitko, J. Mravlje, and K. Haule, Ground state of the parallel double quantum dot system, *Phys. Rev. Lett.* **108**, 066602 (2012).
- [54] In Ref. [40], our Γ_0 , Γ_1 , and t_{01} notation becomes Γ_1 , Γ_2 , and t , respectively.